

A Semiclassical Framework for Mixed Quantum Classical Dynamics

Shreyas Malpathak,¹ Matthew S. Church,² and Nandini Ananth¹

¹*Department of Chemistry and Chemical Biology, Baker Laboratory, Cornell University Ithaca, 14853 NY, USA*

²*Department of Chemistry, Brown University, Providence, RI 02906, USA*

(Dated: 22 July 2022)

Semiclassical approximations for quantum dynamic simulations in complex chemical systems range from rigorously accurate methods that are computationally expensive to methods that exhibit near-classical scaling with system size but are limited in their ability to describe quantum effects. In practical studies of high-dimensional reactions, neither extreme is the best choice: frequently a high-level quantum mechanical description is only required for a handful of modes, while the majority of environment modes that do not play a key role in the reactive event of interest are well served with a lower level of theory. In this feature we introduce Modified Filinov filtration as a powerful tool for mixed quantum-classical simulations in a uniform semiclassical framework.

I. INTRODUCTION

The development of approximate quantum dynamic methods for the simulation of complex reactions remains an outstanding challenge despite several decades of active research. In the search for a rigorous method capable of predictive simulations, approximations based on Semiclassical (SC) theory have emerged as a practical route to the calculation of real-time quantum correlation functions.^{1–17} Classifying SC methods by the extent to which they can capture quantum mechanical behaviors including nonadiabatic effects, deep tunneling, and nuclear coherence, we find a clear trend: the more rigorous, ‘quantum-limit’ approximations are computationally expensive and limited to dynamic calculations in model systems and small molecules, while the less accurate ‘classical-limit’ methods lend themselves to complex system simulations. In order to mitigate this inverse relationship between computational cost and accuracy, several methods have also been developed that further approximate quantum-limit SC approximations, and these have been used to successfully calculate reaction rates^{2,18–29}, compute linear and non-linear spectra^{30–64}, and simulate nonadiabatic dynamics.^{9,10,12,65–95} Despite these advances, rigorous quantum-limit SC studies of high-dimensional chemical systems remains largely out of reach.

Within SC methods, Semiclassical Initial Value Representation (SC-IVR) has, arguably, shown the most sustained promise in the simulation of chemical systems.^{1,9} In the path integral representation of quantum mechanics, the real-time quantum propagator is obtained by summing over the phase contributions of all possible paths connecting an initial and final configuration in time t .⁹⁶ The original Van-Vleck (VV) SC approximation to the propagator is derived using a stationary phase approximation that truncates this sum over all paths to include only paths of stationary action (classical paths) with a prefactor that accounts for contributions from near-classical paths.⁹⁷ However, finding all classical paths between a fixed initial and final configuration is still challenging (the boundary value problem). The IVR framework addresses this by replacing the integrals over fixed final configurations with integrals over initial momenta, reframing the problem as one of sampling initial phase space conditions from which deter-

ministic classical trajectories can be generated.^{98–101} The VV-IVR propagator employs a position-state basis, while using an over-complete coherent state basis results in the popular Herman-Kluk (HK)-IVR approximation to the propagator.¹⁰²

SC-IVR based approximations to real-time quantum correlation functions involve two propagators — one forward in time and one backward in time. Employing the HK-IVR approximation for both propagators, leads to the Double HK (DHK)-IVR approximation to the correlation function, and this method, along with its near-relation the DVV-IVR approximation,¹⁸ represent quantum-limit SC approximations capable of capturing almost all quantum effects in low-dimensional systems.¹ As system dimensionality is increased, both these quantum-limit approximations become computationally intractable due to the infamous SC sign problem. Succinctly, the sign problem refers to the difficulty numerically converging an integral over a multidimensional, rapidly oscillating function. There have been many efforts over the years to mitigate this sign problem in SC theory and here we describe a few strategies employed in the calculation of SC-IVR based approximations to correlation functions.

Computing a quantum-limit correlation function involves generating classical forward and backward trajectories from properly sampled initial conditions, evaluating a complex SC prefactor associated with each trajectory, and then evaluating an oscillatory integrand with a phase that is largely attributed to the difference in action between the forward and backward trajectories. Linearizing in this forward-backward action difference mitigates the sign problem by significantly reducing the oscillatory structure of the integrand and leading to the well established, classical-limit Linearized Semiclassical (LSC)-IVR approximation.^{11,19,20,103,104} However, while LSC-IVR and the related Husimi-IVR,^{105,106} can account for some quantum effects like zero-point energy and shallow tunneling, these methods cannot be used to describe processes where deep tunneling or interference effects play a key role.^{1,11,107} Despite this limitation, LSC-IVR in particular finds extensive application in the calculation of dynamic observables for high-dimensional systems, and in the condensed phase^{21–26,31–34,108–116} where they provide quantum dynamic information at a computational cost comparable to classical molecular dynamics (MD) simulations.

Strategies to mitigate the sign problem while retaining the

ability to capture some interference effects have focused on improved phase space sampling for initial conditions. For instance, it has been shown that correlated sampling the forward and backward trajectory initial conditions or employing a time-dependent sampling function can lead to more rapid convergence of the oscillatory integrand.^{117–121} Similarly, time-averaging (TA)-SC-IVR,^{35–37,122–124} implemented by drawing initial conditions from phase space configurations along a classical trajectory has been shown to significantly improve convergence.³⁵ Other efforts to tame the phase of the oscillatory integrand have resulted in methods like the Forward-Backward IVR^{27,38,107,125–133} that control the extent to which forward and backward trajectories differ rather than linearizing the action to make them coincide. This gives rise to methods that can still capture some coherence effects unlike the classical-limit SC-IVR approximations.¹⁰⁷

The severity of the sign problem increases with the number of system degrees of freedom motivating the development of hybrid/fragment SC methods, where the number of modes that contribute to the overall phase is limited by partitioning the system into subsystems that are then described using different levels of SC (or related) theory. Proposed multi-physics methods include the use of LSC-IVR for the more classical subsystem¹⁰³, combining VV-IVR for the quantum subsystem with a prefactor-free VV-IVR for the rest^{58,59}, and the Semi-classical hybrid dynamics method^{60–64,134–136} that employs HK-IVR for the quantum subsystem and its near-relation, Thawed Gaussian Wavepacket dynamics,^{137–139} for the rest of the system. In general, these multi-physics approaches introduce additional approximations in describing inter-subsystem interactions and work best when this coupling is very weak.

We note that a second computational bottleneck in quantum-limit SC-IVR simulations arises from the complex prefactor that is evaluated by taking the square root of a complex determinant constructed from elements of the Monodromy matrices.^{18,102} The log-derivative prefactor approach side-steps evaluating the complex square root in the HK-IVR prefactor and simplifies the equations of motion considerably.¹⁴⁰ Other methods to reduce the cost of computing the SC prefactor include the Johnson multi-channel approximation,^{39,40,124,141,142} the adiabatic approximation,^{143,144} the so-called poor person’s approximation,¹⁴⁵ and others introduced specifically to deal with chaotic systems.⁴¹ A different approach that circumvents the calculation of pre-factors is the pre-factor-free SC-IVR series approach¹⁴⁶ that is derived from more general SC-IVR series formalism developed systematically to correct for differences between the HK-IVR propagator and the exact quantum propagator^{147–149}. On-the-fly simulations of high dimensional systems have been undertaken in the SC framework, some leveraging both prefactor approximations and a modified implementation of the TA-SC-IVR approach.^{40,42–57}

In this feature, we describe a new SC framework that allows for different degrees of freedom to be treated at different levels of SC theory without introducing any *ad hoc* approximations to capture interactions between them. This is achieved through a mode-specific phase filtration scheme, Modified Filinov Filtration (MFF), that when applied to DHK-IVR effec-

tively controls the extent to which each degrees of freedom contributes to the phase of the integrand. By varying the filter strength, it is possible to limit contributions to the overall phase to a handful of important degrees of freedom, while the rest are treated in the classical-limit, or on a continuum between these two limits. We introduce the derivation of this Mixed Quantum-Classical (MQC)-IVR method and discuss the applications to-date, as well as some of the limitations. We demonstrate that, for linear operator, changing the strength of the phase filter systematically changes the MQC-IVR expression for a real-time correlation function from the quantum-limit DHK-IVR to the classical-limit Husimi IVR.^{150,151} We show numerical results obtained by using this method to characterize the dynamics in multidimensional systems with strong and weak inter-mode coupling,^{150–152} to model multi-channel scattering in nonadiabatic model systems,¹⁵³ and to calculate condensed phase reaction rates.¹⁵² We note the limitations of the MQC-IVR as it currently stands for the evaluation of non-linear operator correlation functions and the computational cost associated with the MQC prefactor. We then introduce a new prefactor-free MQC method obtained by applying MFF to the exact, real-time, path integral expression for correlation functions. The resulting Filinov-Filtered Path Integral (FFPI) expression for the correlation function moves systematically from an exact path integral expression to a classical-limit LSC-IVR correlation function as the phase of the Filinov filter is increased. We conclude by discussing the challenges in sampling path space in this new framework, potential implementation strategies, and more generally, the future of MQC-SC methods.

II. MIXED QUANTUM CLASSICAL INITIAL VALUE REPRESENTATION

As described earlier, the oscillatory phase of the DHK-IVR integrand is primarily due to the action difference between pairs of forward-backward trajectories. This motivates the derivation of the MQC-IVR approximation using MFF to control the extent to which individual degrees of freedom contribute to the action difference, and therefore the overall phase of the DHK-IVR integrand.

A. DHK-IVR approximation for real-time correlation functions

Experimentally measured dynamic observables like time-dependent expectation values, reaction rates, and spectra frequently correspond to real-time quantum correlation functions,

$$C_{AB}(t) = \text{Tr} \left[\hat{A} e^{i\hat{H}t/\hbar} \hat{B} e^{-i\hat{H}t/\hbar} \right], \quad (1)$$

where Tr signifies the trace, \hat{H} is the system Hamiltonian, and \hat{A} and \hat{B} are the operators of interest. For condensed phase systems, the density operator, $\hat{\rho}$, is typically grouped with the observable, $\hat{A}_\rho = \hat{\rho}\hat{A}$.

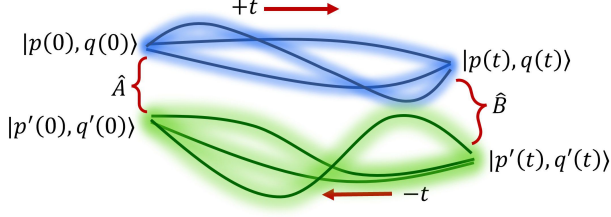


FIG. 1. A schematic showing the structure of a DHK-IVR correlation function $C_{AB}(t)$. The initial coherent state of the system at time zero, $|p_0, q_0\rangle$, is time-evolved forward to state $|p_t, q_t\rangle$. Operator \hat{B} acts on $|p_t, q_t\rangle$ to generate a new state, $|p'_t, q'_t\rangle$, which is then evolved backward in time to a final state, $|p'_0, q'_0\rangle$. Matrix elements of operators \hat{A} and \hat{B} are evaluated at time $t = 0$ and t respectively. The classical paths that contribute to the DHK-IVR integrand are shown with solid lines and the surrounding region highlighted to indicate that the HK prefactor captures contributions from near-classical paths as well.

The DHK-IVR approximation to the real-time quantum correlation function is,

$$C_{AB}^{\text{DHK}}(t) = \frac{1}{(2\pi\hbar)^{2F}} \int d\mathbf{p}_0 \int d\mathbf{q}_0 \int d\mathbf{p}'_t \int d\mathbf{q}'_t C_t(\mathbf{p}_0, \mathbf{q}_0) \times C_{-t}(\mathbf{p}'_t, \mathbf{q}'_t) \langle \mathbf{p}_0 \mathbf{q}_0 | \hat{A} | \mathbf{p}'_0 \mathbf{q}'_0 \rangle \langle \mathbf{p}'_t \mathbf{q}'_t | \hat{B} | \mathbf{p}_t \mathbf{q}_t \rangle \times e^{i[S_t(\mathbf{p}_0, \mathbf{q}_0) + S_{-t}(\mathbf{p}'_t, \mathbf{q}'_t)]/\hbar}, \quad (2)$$

where F is the dimensionality of the system, the forward path is described by initial phase space variables, $(\mathbf{p}_0, \mathbf{q}_0)$, that are time evolved classically to the final variables, $(\mathbf{p}_t, \mathbf{q}_t)$, and backward path defined by inverse time evolution from $(\mathbf{p}'_t, \mathbf{q}'_t)$ to $(\mathbf{p}'_0, \mathbf{q}'_0)$ as sketched in Fig 1. In Eq. 2, the phase of the integrand is determined by the forward-backward action difference, $S_t(\mathbf{p}_0, \mathbf{q}_0) + S_{-t}(\mathbf{p}'_t, \mathbf{q}'_t)$, and the Herman-Kluk prefactor for the forward trajectory defined as

$$C_t^2(\mathbf{p}_0, \mathbf{q}_0) = \det \left| \frac{1}{2} \left[\gamma_t^{\frac{1}{2}} \mathbf{M}_{qq}^f \gamma_0^{-\frac{1}{2}} + \gamma_t^{-\frac{1}{2}} \mathbf{M}_{pp}^f \gamma_0^{\frac{1}{2}} - i\hbar \gamma_t^{\frac{1}{2}} \mathbf{M}_{qp}^f \gamma_0^{\frac{1}{2}} + \frac{i}{\hbar} \gamma_t^{-\frac{1}{2}} \mathbf{M}_{pq}^f \gamma_0^{-\frac{1}{2}} \right] \right|, \quad (3)$$

where $\mathbf{M}_{\alpha\beta}^f = \frac{\partial \alpha_t}{\partial \beta_0}$ are the Monodromy matrices along the forward path, and C_{-t} is similarly defined in terms of backward path Monodromy matrices.¹⁰²

B. Modified Filinov Filtration

Consider the integral over an F -dimensional oscillatory function,

$$I = \int d\mathbf{r} g(\mathbf{r}) e^{i\phi(\mathbf{r})}, \quad (4)$$

where $g(\mathbf{r})$ is, in general, complex-valued and $\phi(\mathbf{r})$ is a real-valued phase. The Modified Filinov filtration (MFF)^{154–156} approximation to the integral in Eq. 4 is

$$I(\mathbf{c}) = \int d\mathbf{r} g(\mathbf{r}) e^{i\phi(\mathbf{r})} F(\mathbf{r}; \mathbf{c}), \quad (5)$$

where $F(\mathbf{r}; \mathbf{c})$ is the smoothing factor,

$$F(\mathbf{r}; \mathbf{c}) = \det \left| \mathbb{1} + i\mathbf{c} \frac{\partial^2 \phi}{\partial \mathbf{r}^2} \right|^{\frac{1}{2}} e^{-\frac{1}{2} \frac{\partial \phi}{\partial \mathbf{r}}^T \cdot \mathbf{c} \cdot \frac{\partial \phi}{\partial \mathbf{r}}}, \quad (6)$$

and elements of the diagonal, $F \times F$, Filinov parameter matrix, \mathbf{c} , determine the strength of the phase filter. When all the Filinov parameters are zero, the integral I in Eq. 5 is identical to the original integrand. In the limit of infinitely large Filinov parameters, it can be shown that $I(\mathbf{c})$ in Eq. 5 corresponds to a stationary phase approximation to the integral in Eq. 4.¹⁵⁵ For finite, non-zero values of the Filinov parameters, the MFF integrand is less oscillatory than the original, and by choosing the elements of the Filinov parameter matrix to be distinct, it becomes possible to tune the extent to which an individual degree of freedom contribute to the overall phase.

C. Deriving MQC-IVR

By filtering the phase of the DHK-IVR integrand using MFF, we obtain the MQC-IVR correlation function,

$$C_{AB}^{\text{MQC}}(t; \mathbf{c}) = \frac{1}{(2\pi\hbar)^{2F}} \int d\mathbf{p}_0 \int d\mathbf{q}_0 \int d\Delta_{p_t} \int d\Delta_{q_t} D(\mathbf{p}_0, \mathbf{q}_0, \Delta_{p_t}, \Delta_{q_t}, \mathbf{c}_p, \mathbf{c}_q) \langle \mathbf{p}_0 \mathbf{q}_0 | \hat{A} | \mathbf{p}'_0 \mathbf{q}'_0 \rangle \times \langle \mathbf{p}'_t \mathbf{q}'_t | \hat{B} | \mathbf{p}_t \mathbf{q}_t \rangle e^{i[S_t(\mathbf{p}_0, \mathbf{q}_0) + S_{-t}(\mathbf{p}'_t, \mathbf{q}'_t)]/\hbar} e^{-\frac{1}{2} \Delta_{q_t}^T \cdot \mathbf{c}_q \cdot \Delta_{q_t}} e^{-\frac{1}{2} \Delta_{p_t}^T \cdot \mathbf{c}_p \cdot \Delta_{p_t}}, \quad (7)$$

where the complex prefactor, D , is defined in Appendix A. As previously discussed, the classical-limit corresponds to forward and backward trajectories that coincide, $\Delta_{p_t} = \Delta_{q_t} = 0$, with net zero action. Trajectory pairs with finite displacements, $\Delta_{p_t} = \mathbf{p}'_t - \mathbf{p}_t$ and $\Delta_{q_t} = \mathbf{q}'_t - \mathbf{q}_t$, contribute a significant non-zero phase $S_t + S_{-t}$. In Eq. 7, we see that the $F \times F$ diagonal Filinov matrices, \mathbf{c}_p and \mathbf{c}_q , parameterize the width of Gaussians in Δ_{p_t} and Δ_{q_t} , respectively, and therefore, determine the types of forward-backward paths that contribute to the overall phase of the MQC-IVR integrand. In the limit $\{\mathbf{c}_p, \mathbf{c}_q\} \rightarrow 0$, Eq. (7) reduces to the DHK-IVR expression Eq. (2) for the correlation function and in the $\{\mathbf{c}_p, \mathbf{c}_q\} \rightarrow \infty$ limit, $\{\Delta_{p_t}, \Delta_{q_t}\} \rightarrow 0$, and for *linear operators* we obtain the classical limit Husimi-IVR expression,¹⁵⁰

$$C_{AB}^{\text{Hus}}(t) = \frac{1}{(2\pi\hbar)^{2F}} \int d\mathbf{p}_0 \int d\mathbf{q}_0 \langle \mathbf{p}_0 \mathbf{q}_0 | \hat{A} | \mathbf{p}'_0 \mathbf{q}'_0 \rangle \times \langle \mathbf{p}'_t \mathbf{q}'_t | \hat{B} | \mathbf{p}_t \mathbf{q}_t \rangle. \quad (8)$$

We note that a previous work applying MFF to DHK-IVR resulted in the Generalized Forward-Backward (GFB)-IVR.¹⁵⁷ Formally, the difference between the GFB-IVR and MQC-IVR correlation functions is simply a matter of the choice of phase to be filtered: MQC-IVR filters only the phase due to the action difference, whereas GFB-IVR also filters phase contributions from the matrix elements of operator \hat{B} . In the zero filter limit, both GFB-IVR and MQC-IVR correspond to DHK-IVR, however, when the Filinov parameter is set to large values, the GFB-IVR correlation function becomes identical to the FB-IVR correlation function, a quantum-limit method in our classification with only marginally improved numerical convergence properties.¹⁵⁷

The implementation of the MQC-IVR correlation function is similar to other quantum-limit SC methods like the DHK-IVR. Trajectory initial conditions are obtained by Monte Carlo sampling initial phase space positions $(\mathbf{p}_0, \mathbf{q}_0)$ for the forward trajectories and the difference variables, $(\Delta_{p_t}, \Delta_{q_t})$, at time t to generate initial conditions for the backward trajectories. Note that this ‘forward-backward’ implementation described here is less efficient than a more recently introduced double-forward (DF) implementation where the phase space variables at time zero, $(\mathbf{p}_0, \mathbf{q}_0, \mathbf{p}'_0, \mathbf{q}'_0)$ are Monte Carlo sampled, allowing for two independent forward trajectories to be generated.¹⁵¹ All MQC-IVR results presented in this article were generated using the SC-Corr code package, an open-source program developed in-house.¹⁵⁸

D. Numerical Study of Phase Filtering in MQC-IVR

The phase filtration achieved in the MQC-IVR framework is best understood and demonstrated with a model system. We choose to work with the real-time position correlation function for a 1D anharmonic oscillator initially in a non-stationary state, where the expected quantum-limit amplitude recurrences are systematically damped as the filter strength is increased and the MQC-IVR correlation function approaches

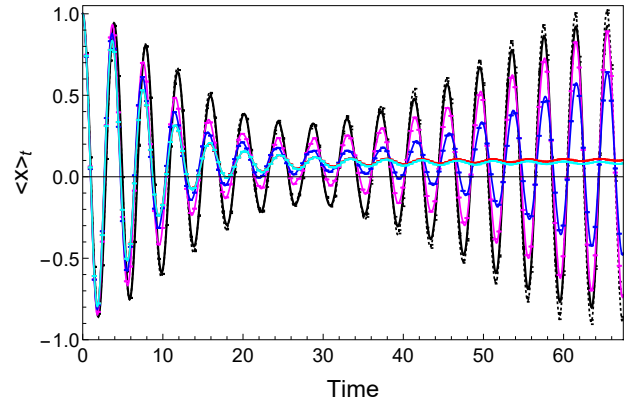


FIG. 2. The exact position correlation function for a 1D anharmonic oscillator, obtained by diagonalizing the Hamiltonian on a Discrete Variable Representation (DVR) grid¹⁵⁹ is shown as a solid black line. DHK-IVR results are plotted with dashed black lines and the classical-limit Husimi-IVR is shown with a red solid line. MQC-IVR correlation function results are shown for different values of the Filinov parameter, $c_p = 0.7$ (pink), $c_p = 3.0$ (blue), $c_p = 500$ (cyan). The plots demonstrate that the amplitude of oscillations at long times moves gradually from the quantum recurrences in DHK-IVR to the fully damped classical limit Husimi-IVR. Figure adapted from Ref. 151.

the classical-limit.¹⁵⁰ Detailed analysis establishes that the Filinov filter effectively acts to reduce noise arising from numerically integrating over regions where the integrand has near-zero amplitude but highly oscillatory phase.¹⁵¹

The specific model details are as follows: a particle of mass $m_x = 1$ a.u. is subject to an anharmonic potential,

$$V(x) = \frac{1}{2}m_x\omega_x x^2 - 0.1x^3 + 0.1x^4 \quad (9)$$

where $\omega_x = \sqrt{2}$ a.u. For the position correlation function, we define operator $\hat{A} \equiv |p_i q_i\rangle \langle p_i q_i|$ and $\hat{B} \equiv \hat{x}$ where the initial coherent state wavefunction is

$$\langle x | p_i q_i \rangle = \left(\frac{\gamma_x}{\pi} \right)^{\frac{1}{4}} e^{-\frac{\gamma_x}{2}(x-q_i)^2 + ip_i(x-q_i)}, \quad (10)$$

with $\gamma_x = \sqrt{2}$, $p_i = 0$ and $q_i = 1$, all in atomic units.

The MQC-IVR position correlation functions obtained for different values of the Filinov parameter are shown in Fig. 2. We note that there is only one Filinov parameter, c_p , in this calculation since operator \hat{B} is a position operator, the change in momentum, Δ_{p_t} , is finite while $\Delta_{q_t} = 0$. As shown in Fig. 2, for small values of this Filinov parameter, MQC-IVR captures long-time quantum recurrence with accuracy comparable to DHK-IVR. As the strength of the Filinov phase filter is increased, the coherent structure is damped and the resulting correlation function coincides with the classical-limit result, specifically the Husimi-IVR.¹⁵¹ Table I demonstrates one of the advantages of the MQC-IVR approach: for finite but near zero values of the Filinov parameter, the number of trajectories required to obtain a converged result shows improvement over the corresponding DHK-IVR simulation, and this number further decreases as the filter strength is increased.

TABLE I. The number of trajectories N_{traj} needed to achieve numerical convergence for calculating the position correlation function with different formulations. Data from Ref. 151

IVR formulation	c_p	N_{traj}
DHK	0	3.0×10^6
	0.7	2.4×10^4
MQC	3.0	9.6×10^3
	500.0	6.0×10^2
Husimi	∞	2.4×10^2

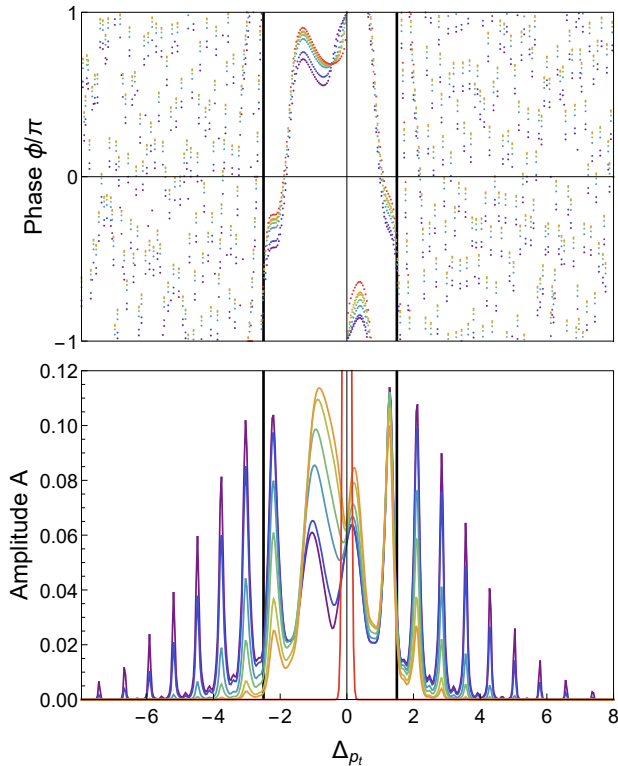


FIG. 3. The phase (top) and amplitude (bottom) contribution to the MQC integrand for the 1D anharmonic oscillator position correlation function generated from a single initial phase space point for the forward trajectory with all possible backward trajectories as a function of Δp_t . In both plots, the colors correspond to different values of the Filinov parameter, $c_p = 0.05$ (purple), $c_p = 0.1$ (blue), $c_p = 0.3$ (blue-green), $c_p = 0.5$ (green), $c_p = 0.7$ (yellow), $c_p = 1.0$ (orange), and $c_p = 200$ (red). The vertical black lines in both plots enclose the regions of slowly varying phase. We find that by increasing the strength of the filter, it is possible to confine the amplitude to have non-zero values only in the region of relatively stationary phase. Figure adapted from Ref. 151.

Careful numerical analysis of the MQC-IVR integrand for the position correlation function shown in Fig. 2 serves to establish the efficacy of the MFF scheme. In Fig. 3 (top), we show the contribution of each pair of forward-backward trajectories to the phase and amplitude of the MQC integrand, as a function of the momentum displacement, Δp_t . We find that there exists a range of Δp_t values that define a region of relatively slowly varying phase, and outside this range, corre-

sponding to larger values of $|\Delta p_t|$, the phase oscillates rapidly. Plotting the amplitude of the integrand for each of these pairs in Fig. 3 (bottom), we find that, in the quantum limit, the small but non-zero amplitudes in regions of highly oscillatory phase result in a very noisy integrand. As the Filinov parameter value is increased, we find that the amplitude is increasingly constrained to be non-zero only in the vicinity of the $\Delta p_t \rightarrow 0$, resulting in a much less oscillatory integrand.¹⁵¹ Having established how changing the filter strength modifies components of the integrand, we examine the phase and amplitude averaged over an ensemble of trajectory pairs. Figure 4 (bottom) shows the amplitude of a small-filter MQC-IVR integrand ensemble averaged over an increasing number of trajectories; as we approach the number required to numerically converge the DHK-IVR integral ($\sim 10^6$), the amplitude in regions of non-stationary phase becomes negligible, but does not completely vanish giving rise to residual noise in the integrand. Overlaying the Filinov filter parameterized Gaussian function in Δp_t over the MQC-IVR integrand in Fig. 4, we find that increasing c_p from the small-filter limit to a larger value ($c_p = 0.7$ in this case) is sufficient to zero amplitude in regions of non-stationary phase, reducing the noise in the integrand, and allowing for more rapid numerical convergence without significant loss in accuracy.

E. Nonadiabatic MQC-IVR

Nonadiabatic dynamic processes, where nuclear motion is coupled to and drives transitions between electronic states, have been studied using a variety of SC-IVR methods.^{9,10,12,65–73,75–95} This is facilitated by the Meyer-Miller-Stock-Thoss (MMST) mapping^{160,161} where discrete electronic state variables are mapped to continuous Cartesian electronic phase space variables that can undergo approximate time-evolution under a classical analog Hamiltonian. Using the MMST mapping, a nonadiabatic MQC-IVR expression can be derived to enable independent control over the extent of quantization of the nuclear and electronic degrees of freedom.¹⁵³ In addition, a novel symplectic integration scheme has been proposed to enable accurate time evolution of the nuclear and electronic degrees of freedom as well as the Monodromy matrices that appear in the MQC prefactor.^{153,162}

F. Analytic Mixed Limit MQC-IVR

Although choosing a small but non-zero value of the Filinov parameter can offer a significant mitigation of the sign problem in low-dimensional systems, for complex system studies, it is expedient to simply choose a handful of degrees of freedom to describe in the quantum limit while treating the rest of the system in the classical limit. This motivates the derivation of an analytic, mixed-limit AMQC-IVR correlation func-

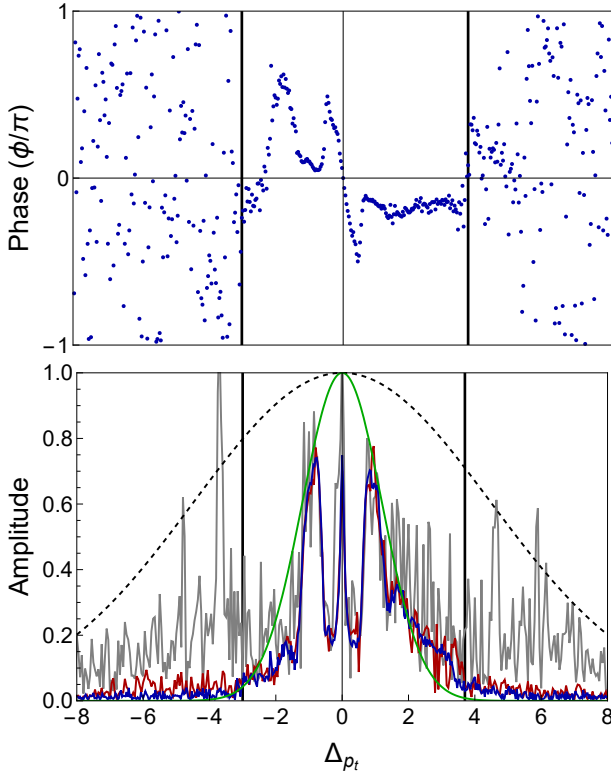


FIG. 4. The phase (top) and amplitude (bottom) of the MQC-IVR integrand for the position correlation function are plotted against the momentum displacement between forward-backward trajectories in the quantum limit, ensemble averaged over 1.2×10^3 trajectories (gray), 6.0×10^4 trajectories (red), and 2.4×10^5 trajectories (blue). Overlaid on the amplitude plot, we also show the Filinov filter Gaussians using a black dashed line for the weak filter ($c_p = 0.05$) and a green dashed-line for the ‘optimal’ filter strength ($c_p = 0.7$). Figure adapted from Ref. 151.

tion,¹⁵²

$$\begin{aligned}
C_{AB}^{\text{AMQC}}(t) &= \frac{1}{(2\pi\hbar)^{F+F_Q}} \int d\mathbf{p}_0 \int d\mathbf{q}_0 \int d\mathbf{p}'_Q \int d\mathbf{q}'_Q \\
&\times C_t(\mathbf{p}_0, \mathbf{q}_0) C_t^*(\mathbf{p}'_Q, \mathbf{q}'_Q) \langle \mathbf{p}_0 \mathbf{q}_0 | \hat{A} | \mathbf{p}'_Q \mathbf{q}'_Q \rangle \\
&\times \langle \mathbf{p}'_Q \mathbf{q}'_Q | \hat{B} | \mathbf{p}_t \mathbf{q}_t \rangle e^{i[S_t(\mathbf{p}_0, \mathbf{q}_0) - S_t(\mathbf{p}'_Q, \mathbf{q}'_Q)]/\hbar} \\
&\times \Lambda_t(\mathbf{p}_0, \mathbf{q}_0, \mathbf{p}'_Q, \mathbf{q}'_Q), \quad (11)
\end{aligned}$$

where F is the total system degrees of freedom (dofs), $(\mathbf{p}_0, \mathbf{q}_0)$ are F -dimensional position and momentum vectors, F_Q is the number of quantized dofs for which the Filinov parameters are set to exactly zero, and $(\mathbf{p}'_Q, \mathbf{q}'_Q)$ are the phase space variables of the subset of quantized dofs. The AMQC-IVR prefactor in Eq. 11 is the product of the F_Q dimensional HK-IVR prefactors corresponding to the forward (C_t) and backward (C_t^*) propagators, and Λ_t represents an F dimensional determinant corresponding to coupling between the quantum and classical dofs, defined in detail in Ref. 152. In the limit where the quantum subsystem is only weakly coupled to the rest of the system, a further separable prefactor approximation can be made

by setting $\Lambda_t = 1$.¹⁵²

G. MQC-IVR Results and Discussion

The quantum interference pattern obtained when a particle is incident upon a screen with two slits, the double slit experiment, highlights the non-additive nature of probability in quantum mechanics and serves as our first test-case for MQC-IVR. Specifically, we use MQC-IVR to obtain the probability distribution for particle subject to a quantum double-slit experiment mimicked by a 2D Hamiltonian,¹⁰⁷

$$H = \frac{p_x^2}{2m} + \frac{p_y^2}{2m} + \left(\bar{V} - \frac{1}{2} m \omega^2 y^2 + \frac{m^2 \omega^4 y^4}{16\bar{V}} \right) e^{-(x/\alpha)^2}, \quad (12)$$

with $m = 1$ a.u., $\alpha = 50$ a.u., $\omega = 600$ cm⁻¹ and $\bar{V} = 8000$ cm⁻¹. The initial wavefunction is a 2D coherent state,

$$\begin{aligned}
\langle x, y | \psi_i \rangle &= \left(\frac{\gamma_x \gamma_y}{\pi^2} \right)^{\frac{1}{4}} e^{-\frac{\gamma_x}{2}(x-q_x)^2 + i p_x(x-q_x)} \\
&\times e^{-\frac{\gamma_y}{2}(y-q_y)^2 + i p_y(y-q_y)}, \quad (13)
\end{aligned}$$

with parameters $\gamma_x = 1/2\alpha^2$ and $\gamma_y = m\omega^2/8V_0$, initial positions centered at $q_x = -220$ a.u. and $q_y = 0$ a.u., and initial momenta centered at $p_y = 0$ a.u., and $p_x^2/2m = 2048$ cm⁻¹, where the positive sign indicates motion in the direction of the double slit. The double slit potential is plotted in Fig. 5 along with the initial wavepacket with average energy significantly less than the barrier height to ensure that the particle must pass through the slits.

The MQC-IVR angular distributions obtained as the long time limit of a real-time correlation function with $\hat{A} \equiv |\psi_i\rangle \langle \psi_i|$ and $\hat{B} \equiv \delta(\theta_f - \hat{\theta})$ are shown in Fig. 5. For small values of the Filinov parameter, the MQC-IVR integrand includes pair of forward-backward paths where the particle can pass through different slits giving rise to the quantum interference pattern. In the classical strong filter limit, the MQC-IVR correlation function is dominated by contributions from forward and backward paths that are close together, requiring the particle pass through the same slit, collapsing the interference pattern to a classical binodal distribution.

A key feature of MQC-IVR is the ability to treat certain degrees of freedom in the quantum limit and others in the classical limit. We numerically demonstrate this for a 2D potential constructed by coupling the 1D anharmonic oscillator previously defined in Eq. 9 to a heavy harmonic oscillator mode,

$$V(x, y) = \frac{1}{2} m_x \omega_x^2 x^2 - 0.1x^3 + 0.1x^4 + \frac{1}{2} m_y \omega_y^2 y^2 + kxy \quad (14)$$

where $m_x = 1$, $m_y = 25$, $\omega_x = \sqrt{2}$, $\omega_y = 1/3$ and $k = 2.0$ in atomic units. In Fig. 6, we show the MQC-IVR position correlation function for the anharmonic mode, where $\hat{A} \equiv |\psi_i\rangle \langle \psi_i|$ and $\hat{B} \equiv \hat{x}$ compared against exact, DHK-IVR, and Husimi-IVR results. As expected, MQC-IVR results with both c_x and c_y set to low values show good agreement with DHK-IVR, and the results generated with large value Filinov parameters

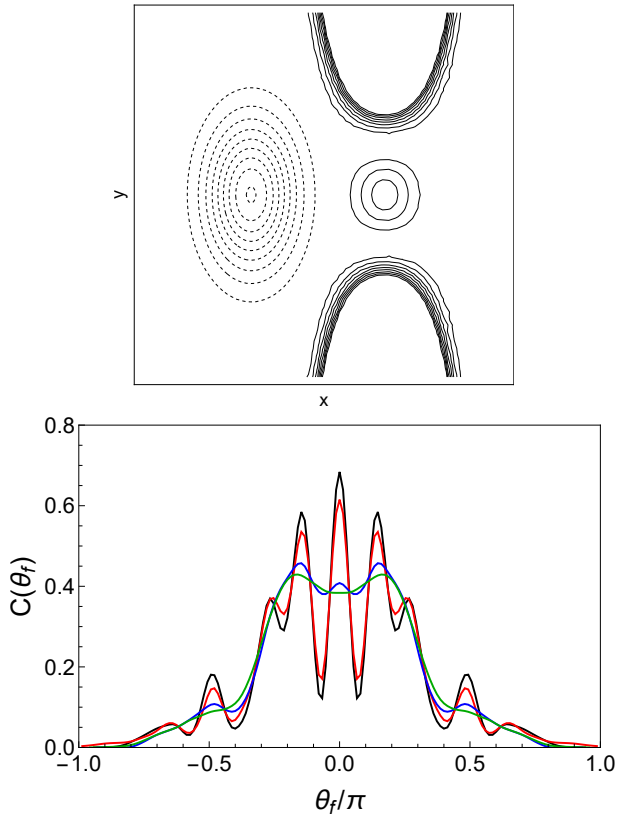


FIG. 5. The potential (top) for the double-slit Hamiltonian is shown as a contour plot with solid black lines and the initial wavepacket density is plotted with black dashed lines. The angular distribution (bottom) calculated using MQC-IVR with $c_x = c_y = 1 \times 10^{-6}$ (black), $c_x = c_y = 1 \times 10^{-5}$ (red), $c_x = c_y = 1 \times 10^{-4}$ (blue), $c_x = c_y = 5 \times 10^{-4}$ (green). We see the interference pattern observed in the quantum limit changes to the classical scattering result as the value of the Filinov parameter is increased.

for both degrees of freedom agree well with the Husimi-IVR correlation function. Interestingly, we find that a mixed limit calculation where only the anharmonic mode is treated in the quantum limit yields results that are nearly indistinguishable from DHK-IVR, and with far fewer trajectories as shown in Table II.

We note that operator \hat{B} appears to play an important role in determining which degree of freedom should be treated in the quantum limit. In Fig 6, $\hat{B} \equiv \hat{x}$, so at time t the operator induces a momentum jump in the anharmonic (x) dimension, suggesting that treating only the anharmonic mode in the quantum limit is sufficient to achieve good agreement with exact quantum results. Similarly, it has been shown that for this same model system when $\hat{B} \equiv \hat{y}$, it is possible to achieve good agreement with the exact quantum correlation function by quantizing only the heavier harmonic (y) degree of freedom.¹⁵⁰ This leads us to conclude that there is not an inherent need to treat specific modes as more or less quantum, rather the observable determines the necessary level of theory.

The importance of the observable is also highlighted in a study of nonadiabatic dynamics, where the electronic states

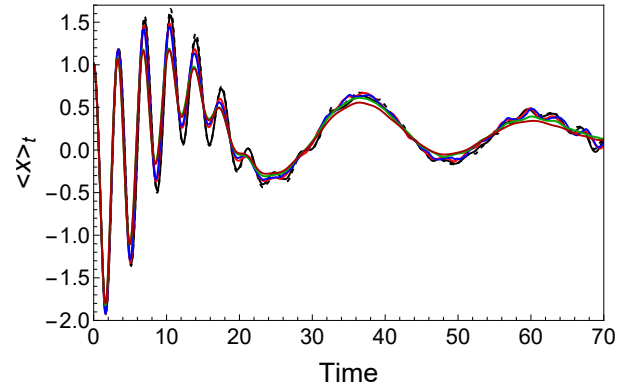


FIG. 6. The x -mode position correlation function for a 2D model system obtained from DVR (solid black), DHK-IVR (dashed black), MQC-IVR with $c_x = 0.2, c_y = 0.2$ (red), $c_x = 0.2, c_y = 50$ (blue), $c_x = 50, c_y = 50$ (green), and Husimi-IVR (brown).

TABLE II. The number of trajectories N_{traj} required establish numerical convergence for the x -mode position correlation function of a 2D model system with different levels of SC theory.

IVR formulation	c_x	c_y	N_{traj}
DHK	0	0	6×10^6
	0.2	0.2	4×10^6
DF-MQC	0.2	50	1×10^6
	50	50	2×10^5
Husimi	∞	∞	8×10^4

are strongly coupled to nuclear degrees of freedom. Specifically, we calculate the final nuclear momentum distribution when a particle is transmitted through a scattering potential pictured in Fig. 7 where two diabatic electronic states are coupled to a single nuclear degree of freedom.¹⁵³ The MQC-IVR correlation function is obtained by histogramming the final nuclear momentum with operator $\hat{B} = \delta(\hat{P} - P_f)$. This model is particularly interesting because previous studies have established that the classical limit LSC-IVR simulations reproduce the various electronic state population correlation functions reasonably accurately,⁹² however, quantum limit methods like DHK-IVR are necessary to correctly capture the final nuclear momentum distribution.⁷⁴

In Fig. 8, we show the final nuclear momentum distribution from MQC-IVR simulations with different values of the Filinov parameter.¹⁵² When the Filinov parameters for all degrees of freedom are tuned from the quantum to the classical limit, we find the expected momentum distribution corresponding to two scattering channels collapses to a single, broad, 'mean-field' like distribution in Fig. 8a. Following our previous observation that the extent of quantization is tied to the degree of freedom directly perturbed by operator \hat{B} , Fig. 8b presents the distributions obtained when the nuclear degree of freedom is treated in the quantum limit, while the Filinov filter is increased systematically for the electronic degrees of freedom. In this mixed limit, we find that although treating the electronic modes in the classical limit introduces additional spuri-

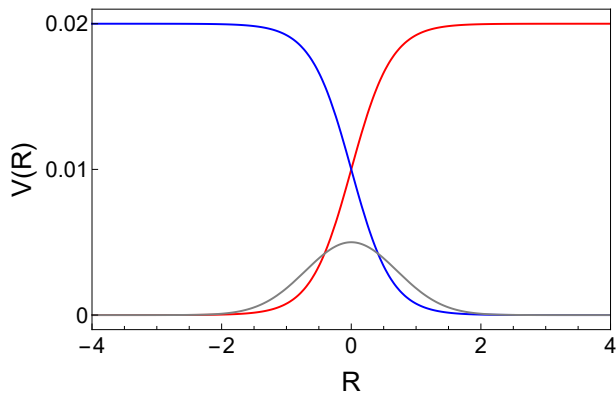


FIG. 7. Elements of the scattering potential, showing the diabatic potential energy matrix elements corresponding to electronic state 1 in red, electronic state 2 in blue, and the coupling between states is shown in grey.

ous peaks in the MQC distribution, it does not cause the distribution to collapse completely to a mean-field result. Conversely, when the electronic degrees of freedom are treated in the quantum limit and the nuclear Filinov parameter increased to the classical-limit, we see the distribution collapse to the mean-field result. This serves to demonstrate that the choice of operator \hat{B} does indeed play an important role in the choice of mode(s) to treat in the quantum limit, however, it is best to treat all strongly coupled degrees of freedom at the same level of theory.

We finish our exploration of the role of operators, coupling, and mixed quantization with AMQC-IVR simulations of high-dimensional system-bath models where the system modes are treated in the analytic quantum limit and the remaining bath modes treated in the classical limit.¹⁵² We calculate the AMQC-IVR anharmonic-mode position correlation function for a system-bath model where an anharmonic oscillator is bilinearly coupled to a bath with an ohmic spectral density and an exponential cut-off,¹⁵²

$$V(x, \mathbf{y}) = \frac{1}{2}m\omega^2x^2 - 0.1x^3 + 0.1x^4 + \sum_{j=1}^N \left[\frac{1}{2}m_j\omega_j^2 \left(y_j^2 - \frac{c_jx}{m_j\omega_j^2} \right)^2 \right], \quad (15)$$

where the number of discretized bath modes $N = 12$.

For very weak system-bath coupling, in Fig. 9, we show that the AMQC-IVR results agree well with the exact quantum results for an uncoupled 1D anharmonic oscillator. As the coupling to the bath is increased, we see the expected damping in oscillatory structure in the AMQC-IVR results.¹⁵² We further investigate the applicability of the separable prefactor approximation that is considerably less expensive, requiring only the SC prefactor be computed for the single system degrees of freedom in Fig. 9. We find that as the coupling to the bath is increased, the separable prefactor approximations begins to fail showing larger deviations from the AMQC-IVR result.¹⁵² Interestingly, we find that the classical limit Husimi

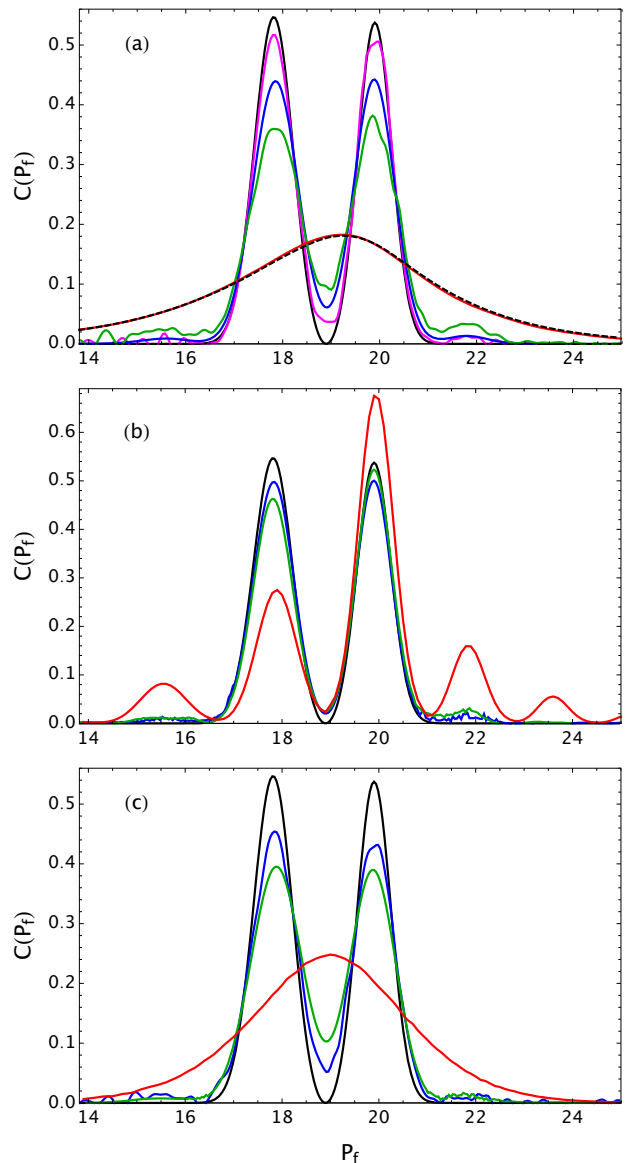


FIG. 8. Final nuclear momentum distribution for a particle incident on the scattering potential pictured in Fig. 7 with initial energy 0.1 a.u. The exact quantum result (black, solid) is shown in each panel along with (a) the Husimi-IVR (black, dashed) and MQC-IVR where the Filinov filter strength for the nuclear and electronic degrees of freedom is set to be equal and to take values ranging from $c = 0.01$ (pink), $c = 0.05$ (blue), $c = 0.1$ (green), to $c = 10.0$ (red). (b) Mixed MQC-IVR simulation results where the nuclear degree of freedom is treated in the quantum limit, $c_{nuc} = 0.01$, and the level of theory to describe electronic states is varied from the quantum limit to the classical limit, with $c_{el} = 0.05$ (blue), $c_{el} = 0.1$ (green), and $c_{el} = 10.0$ (red) (c) Mixed MQC-IVR simulation results where the electronic states are treated in the quantum limit, $c_{el} = 0.01$, and the level of theory for the nuclear degree of freedom is varied from the quantum limit to the classical limit, with $c_{nuc} = 0.05$ (blue), $c_{nuc} = 0.1$ (green), and $c_{nuc} = 10.0$ (red). Figure adapted from Ref. 153.

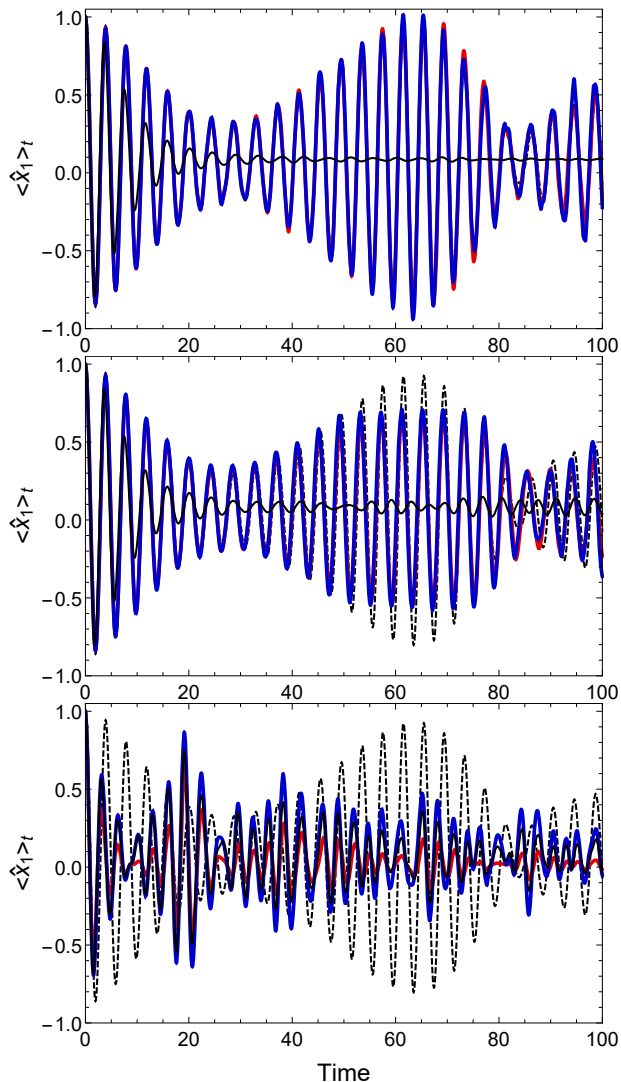


FIG. 9. The position correlation function, $\langle x_1 \rangle_t$ for a system-bath model with potential Eq. (15), calculated using AMQC-IVR (blue), AMQC-IVR with SP approx. (red), and Husimi-IVR (solid black). The coupling strength is $\eta/m\omega_1 = 10^{-4}$ (top), $\eta/m\omega_1 = 10^{-2}$ (middle), and $\eta/m\omega_1 = 1.0$ (bottom). The dotted black line is the exact quantum average position of the 1d anharmonic oscillator uncoupled from the bath. Results adapted from Ref. 152.

IVR results agree better with AMQC-IVR than the separable prefactor approximation, suggesting again that an even-handed treatment of all modes is preferable in the presence of strong coupling.¹⁵²

Finally, we calculate the thermal transmission coefficient, $\kappa(T)$, from the flux-side correlation function for a proton transfer model system comprising a symmetric double well coupled to a bath of harmonic oscillators with an ohmic spectral density and exponential cut-off.¹⁶³ The results from

AMQC-IVR are compared against exact real-time path integral simulations in Fig. 10 showing good agreement for a wide range of system-bath couplings. We note that this study also explored the applicability of the separable prefactor approximation and found it to be valid only in the very weak-coupling

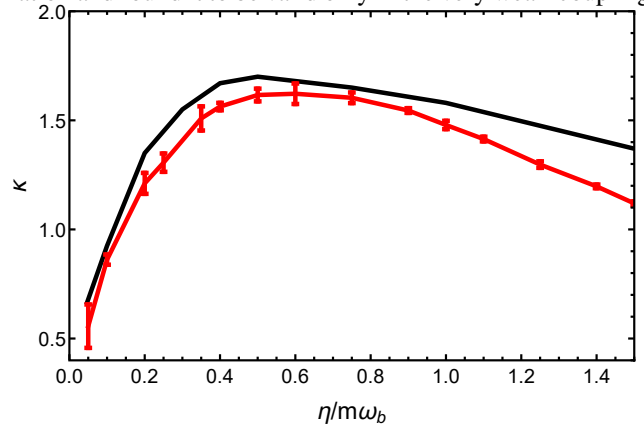


FIG. 10. The thermal transmission coefficient at $T = 300\text{K}$ for a proton-transfer model where a 1D double well potential (system) is coupled to a bath of harmonic oscillators as a function of system-bath coupling calculated using AMQC-IVR (red) compared against exact path integral result (black) generated using the Quasi-Adiabatic Path Integral method.¹⁶³ Figure adapted from Ref. 152.

regime.¹⁵²

H. A Better Path: Filinov Filtered Path Integrals

It is evident that MQC-IVR and AMQC-IVR retain the accuracy of quantum limit SC methods like DHK-IVR while offering a significant reduction in computational effort. The prefactor remains, perhaps, the only limitation in extending these methods to truly complex system simulations: it is necessary to ensure continuity in evaluating the square root of the complex prefactor, and time evolving the prefactor requires knowledge of the Hessian. In this section, we propose an alternate use of the modified Filinov filter to control the extent of oscillatory phase in a real-time correlation function expression. Specifically, rather than starting with a quantum limit SC expression with a prefactor like the DHK-IVR, we derive an expression to filter the phase of an exact real-time path integral correlation function. Note that this derivation takes its inspiration from previous work deriving LSC-IVR by linearizing the forward-backward paths in an exact real-time path integral expression for correlation functions.¹⁰⁴

The path integral expression for a correlation function is obtained by discretizing the forward and backward time evolution operators by inserting identity in position space, and evaluating the resulting short-time propagator matrix elements to obtain,⁹⁶

$$\begin{aligned}
C_{AB}(t) &= \text{Tr} \left[\hat{A} e^{i\hat{H}t/\hbar} \hat{B} e^{-i\hat{H}t/\hbar} \right] = \int dx_0^+ \int dx_0^- \int dx_N^+ \int dx_N^- \langle x_0^+ | \hat{A} | x_0^- \rangle \langle x_0^- | e^{i\hat{H}t/\hbar} | x_N^- \rangle \langle x_N^- | \hat{B} | x_N^+ \rangle \langle x_N^+ | e^{-i\hat{H}t/\hbar} | x_0^+ \rangle \\
&= \lim_{N \rightarrow \infty} \left(\frac{m}{2\pi\hbar\varepsilon} \right)^N \int dx_0^+ \dots \int dx_N^+ \int dx_0^- \dots \int dx_N^- \langle x_0^+ | \hat{A} | x_0^- \rangle \langle x_N^- | \hat{B} | x_N^+ \rangle e^{\frac{i}{\hbar}(S_N^+ - S_N^-)}. \tag{16}
\end{aligned}$$

In Eq. 16, Tr signifies the trace, \hat{H} is the system Hamiltonian, N is the number of time slices, $\varepsilon = t/N$, x_0^\pm and x_N^\pm are the initial and final positions for the forward/backward path, and S_N^\pm represent the action corresponding to the forward/backward paths respectively. Rewriting Eq. (16) in terms of mean (y) and difference (z) path variables we obtain

$$C_{AB}(t) = \lim_{N \rightarrow \infty} \left(\frac{m}{2\pi\hbar\varepsilon} \right)^N \int dy_0 \dots \int dy_N \int dz_0 \dots \int dz_N \langle y_0 + \frac{z_0}{2} | \hat{A} | y_0 - \frac{z_0}{2} \rangle \langle y_N - \frac{z_N}{2} | \hat{B} | y_N + \frac{z_N}{2} \rangle e^{i(S_N^+ - S_N^-)/\hbar}, \tag{17}$$

where

$$y_j = \frac{1}{2} (x_j^+ + x_j^-) \quad \text{and} \quad z_j = x_j^+ - x_j^-, \tag{18}$$

and x_j^\pm are positions corresponding to the j^{th} time slice along the forward/backward paths. The phase due to action difference between the forward and backward paths can also be expressed in mean and difference variables,

$$\begin{aligned}
S_N^+ - S_N^- &= \varepsilon \left[\sum_{j=1}^{N-1} -\frac{m}{\varepsilon^2} (y_{j+1} - 2y_j + y_{j-1}) z_j - \left(V(y_j + \frac{z_j}{2}) - V(y_j - \frac{z_j}{2}) \right) \right. \\
&\quad \left. - \frac{m}{\varepsilon^2} (y_1 - y_0) z_0 - \frac{1}{2} \left(V(y_0 + \frac{z_0}{2}) - V(y_0 - \frac{z_0}{2}) \right) + \frac{m}{\varepsilon^2} (y_N - y_{N-1}) z_N - \frac{1}{2} \left(V(y_N + \frac{z_N}{2}) - V(y_N - \frac{z_N}{2}) \right) \right] \tag{19}
\end{aligned}$$

$$\begin{aligned}
&= \varepsilon \left[\sum_{j=1}^{N-1} z_j \left\{ -\frac{m}{\varepsilon^2} (y_{j+1} - 2y_j + y_{j-1}) - (V'(y_j) + V'''(y_j) \frac{z_j^2}{24} \dots) \right\} \right. \\
&\quad \left. + z_0 \left\{ -\frac{m}{\varepsilon^2} (y_1 - y_0) - \frac{1}{2} (V'(y_0) + V'''(y_0) \frac{z_0^2}{24} \dots) \right\} + z_N \left\{ \frac{m}{\varepsilon^2} (y_N - y_{N-1}) - \frac{1}{2} (V'(y_N) + V'''(y_N) \frac{z_N^2}{24} \dots) \right\} \right], \tag{20}
\end{aligned}$$

where Eq. (20) is obtained by expanding the potential terms in Eq. (19) around y_j . We note that the derivation up to this point follows earlier work establishing a direct derivation of LSC-IVR from an exact path integral expression for a correlation function.¹⁰⁴

We can now employ the MFF scheme to filter the oscillatory integral in Eq. 16 with some care. In the limit of a large filter strength, the MFF scheme is equivalent to a stationary phase approximation; it is evident that if we choose to filter the phase due to the action difference, $S_N^+ - S_N^-$, in Eq. (19) in the limit of $c \rightarrow \infty$ we will obtain the semiclassical DVV-IVR expression. The classical-limit LSC-IVR expression can be obtained in the $c \rightarrow \infty$ limit, if we choose to filter only a portion of the phase,

$$\begin{aligned}
\phi(\mathbf{r}) &= -\frac{1}{\hbar} \sum_{j=1}^{N-1} \left[\frac{m}{\varepsilon} (y_{j+1} - 2y_j + y_{j-1}) + \varepsilon V'(y_j) \right] z_j \\
&= -\frac{1}{\hbar} \sum_{j=1}^{N-1} f_j z_j, \tag{21}
\end{aligned}$$

where $f_j = \frac{m}{\varepsilon} (y_{j+1} - 2y_j + y_{j-1}) + \varepsilon V'(y_j)$ and $\mathbf{r} = \{f_1, z_1, f_2, z_2, \dots, f_{N-1}, z_{N-1}\}$.

Evaluating the first derivative of the phase and using the

definition in Eq. (6), we obtain the Filinov smoothing factor,

$$F(\mathbf{r}; \mathbf{c}) = \prod_{j=1}^{N-1} \left(1 + \frac{c_{z_j} c_{f_j}}{\hbar^2} \right)^{\frac{1}{2}} e^{-\frac{c_{z_j} z_j^2}{2\hbar^2}} e^{-\frac{c_{f_j} f_j^2}{2\hbar^2}}. \tag{22}$$

and the Filinov Filtered Path Integral (FFPI) expression for the correlation function,

$$\begin{aligned}
C_{AB}^{\text{FFPI}}(t; \mathbf{c}) &= \lim_{N \rightarrow \infty} \left(\frac{m}{2\pi\hbar\varepsilon} \right)^N \int dy_0 \dots \int dy_N \int dz_0 \dots \int dz_N \\
&\quad \times \langle y_0 + \frac{z_0}{2} | \hat{A} | y_0 - \frac{z_0}{2} \rangle \langle y_N - \frac{z_N}{2} | \hat{B} | y_N + \frac{z_N}{2} \rangle \\
&\quad \times e^{i(S_N^+ - S_N^-)/\hbar} \prod_{j=1}^{N-1} \left(1 + \frac{c_{z_j} c_{f_j}}{\hbar^2} \right)^{\frac{1}{2}} e^{-\frac{c_{z_j} z_j^2}{2\hbar^2}} e^{-\frac{c_{f_j} f_j^2}{2\hbar^2}}. \tag{23}
\end{aligned}$$

Additional derivation details are provided in Appendix B.

The FFPI correlation function in Eq. 23 contains no SC prefactor, however, the summation runs over *all* forward and backwards paths (expressed in mean and difference variables), unlike in the SC approximation where only classical and near-classical path contributions are included.

In the limit that the Filinov parameter goes to zero, the FFPI correlation function in Eq. (23) becomes the exact path inte-

gral expression for the correlation function. In the classical limit, $\mathbf{c} \rightarrow \infty$, the smoothing factor simplifies to

$$\begin{aligned} \lim_{\mathbf{c} \rightarrow \infty} F(\mathbf{r}; \mathbf{c}) &= \lim_{\mathbf{c} \rightarrow \infty} \prod_{j=1}^{N-1} \left(1 + \frac{c_{z_j} c_{f_j}}{\hbar^2} \right)^{\frac{1}{2}} e^{-\frac{c_{z_j} z_j^2}{2\hbar^2}} e^{-\frac{c_{f_j} f_j^2}{2\hbar^2}} \\ &= (2\pi\hbar)^{N-1} \prod_{j=1}^{N-1} \delta(z_j) \delta(f_j), \end{aligned} \quad (24)$$

and the delta function in f_j corresponds to constraining the mean variable to a classical path,

$$\lim_{\varepsilon \rightarrow 0} \prod_{j=1}^{N-1} \delta(f_j) \implies \frac{d^2}{dt^2} y(t) = -V'[y(t)], \quad (25)$$

where $\varepsilon \rightarrow 0$ or alternatively, $N \rightarrow \infty$. The delta function in z_j ensures that the forward and backward paths coincide. Physically, these two constraints describe the LSC-IVR approximation, and it can be shown that in the classical limit, the FFPI expression becomes identical to LSC-IVR,

$$\begin{aligned} \lim_{\mathbf{c} \rightarrow \infty} C_{AB}^{\text{FFPI}}(t) &= \lim_{N \rightarrow \infty} \left(\frac{m^N}{2\pi\hbar\varepsilon^N} \right) \int dy_0 \dots \int dy_N \int dz_0 \dots \int dz_N \left\langle y_0 + \frac{z_0}{2} \left| \hat{A} \right| y_0 - \frac{z_0}{2} \right\rangle \left\langle y_N - \frac{z_N}{2} \left| \hat{B} \right| y_N + \frac{z_N}{2} \right\rangle e^{i(S_N^+ - S_N^-)} \\ &\times \prod_{j=1}^{N-1} \delta(z_j) \delta(f_j) \end{aligned} \quad (26)$$

$$\begin{aligned} &= \lim_{N \rightarrow \infty} \frac{m^N}{2\pi\hbar\varepsilon^N} \int dy_0 \int dy_N \int dz_0 \dots \int dz_N \int df_1 \dots \int df_{N-1} \left| \frac{\partial \mathbf{y}}{\partial \mathbf{f}} \right| \left\langle y_0 + \frac{z_0}{2} \left| \hat{A} \right| y_0 - \frac{z_0}{2} \right\rangle \\ &\times \left\langle y_N - \frac{z_N}{2} \left| \hat{B} \right| y_N + \frac{z_N}{2} \right\rangle e^{i(S_N^+ - S_N^-)} \prod_{j=1}^{N-1} \delta(z_j) \delta(f_j) \end{aligned} \quad (27)$$

$$= \frac{1}{2\pi\hbar} \int dy_0 \int dy_N \int dz_0 \int dz_N \left| \frac{\partial p_0}{\partial y_N} \right| \left\langle y_0 + \frac{z_0}{2} \left| \hat{A} \right| y_0 - \frac{z_0}{2} \right\rangle \left\langle y_N - \frac{z_N}{2} \left| \hat{B} \right| y_N + \frac{z_N}{2} \right\rangle e^{-\frac{i}{\hbar} p_0 z_0} e^{\frac{i}{\hbar} p_N z_N} \quad (28)$$

$$= (2\pi\hbar)^{-1} \int dy_0 \int dp_0 A_W(y_0, p_0) B_W(y_N, p_N). \quad (29)$$

We obtain Eq. (28) from Eq. (27) by evaluating the delta function integrals over $f_1 \dots f_N$ and $z_1 \dots z_N$, simplifying the action difference,

$$\lim_{N \rightarrow \infty} (S_N^+ - S_N^-) = -p_0 z_0 + p_N z_N, \quad (30)$$

and using the derivative identity

$$\lim_{\varepsilon \rightarrow 0} \left(\frac{m}{\varepsilon} \right)^N \left| \frac{\partial \mathbf{y}}{\partial \mathbf{f}} \right| = \left| \frac{\partial p_0}{\partial y_N} \right|, \quad (31)$$

where we define the vectors $\mathbf{y} = \{y_1, \dots, y_{N-1}\}$ and $\mathbf{f} = \{f_1, \dots, f_{N-1}\}$, and we introduce momentum variables p_j conjugate to positions y_j . Equation (29) is the LSC-IVR correlation function, where we use standard notation O_W to represent the Wigner transform of the corresponding operator \hat{O} .

For finite, non-zero values of the filinov parameters, the FFPI correlation function in Eq. (23) must be evaluated by sampling *all* paths that go from (y_0, z_0) to (y_N, z_N) in time t . Numerically demonstrating the systematic filtration achieved in the FFPI framework is challenging because in one limit, we must sample all paths and in the other limit we must sample only the classical paths associated with the mean-variable. We start by diagonalizing the Hamiltonian matrix on a standard DVR grid¹⁵⁹ to evaluate the short-time matrix elements that comprise the exact real-time path integral correlation func-

tion. The exact path integral result is then obtained by multiplying these short-time matrix elements and summing over all possible intervening grid points. For finite values of the Filinov parameter, we multiply by the Filinov smoothing factor defined in Eq. 22. In Fig. 11, we plot the position correlation function for a 1D anharmonic oscillator previously studied using MQC-IVR. We show that as the Filinov parameter is increased, we see quantum recurrence amplitudes decrease as expected. However, as expected this implementation cannot be used to obtain the numerical classical limit, with the results showing a mismatch in both frequency and amplitude compared with the LSC-IVR result. This is easily understood: the Filinov smoothing factor in the classical limit corresponds to very narrow Gaussians, and correctly implementing this requires converging the grid to a density approaching the continuum. In addition, we recognize that although DVR matrix multiplication offers a way to numerically validate the FFPI correlation function expression, it is not scalable to realistic systems. This motivates the pursuit of a classical trajectory based approach that reproduces the LSC-IVR limit and can perhaps, go beyond to capture some quantum coherences.

In developing such a classical trajectory based implementation, we first classify the space of all paths into three types: (i) Classical paths in the mean variable, $y(t)$, that have $f_j = z_j = 0$ for all j , and that contribute in the $\mathbf{c} \rightarrow \infty$ or LSC-IVR limit. (ii) Pairs of classical forward and backward paths, $x^\pm(t)$ and

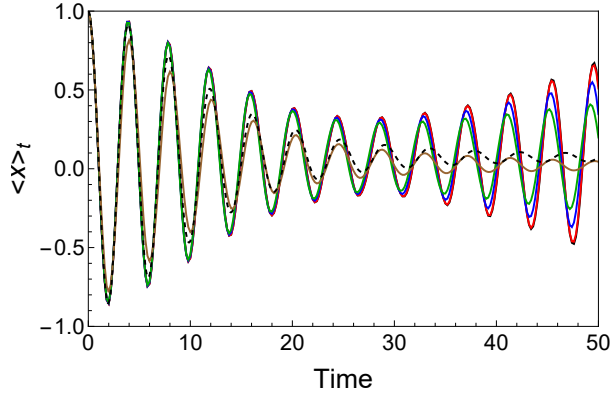


FIG. 11. The position correlation function for a 1D anharmonic oscillator obtained from exact real-time path integrals is shown in black, LSC-IVR results are the black dashed line, and FFPI correlation function results from our DVR implementation with $c = 10^{-4}$ shown in red, $c = 10^{-3}$ shown in blue, $c = 2 \times 10^{-3}$ shown in green, and $c = 4 \times 10^{-3}$ shown in brown. We find that while agreement in the quantum limit is good, for larger values of the Filinov parameter there is significant deviation in the frequency of oscillations from the LSC-IVR result.

$x^-(t)$ respectively. These are the paths that are explicitly generated when performing quantum-limit SC calculations. Rewriting the forward-backward paths in terms of the mean and difference variables, it can be shown that the corresponding $y(t)$ and $z(t)$ dynamics correspond to classical dynamics under an effective potential with $f_j \neq 0$ and $z_j \neq 0$. (iii) All other ‘non-classical’ paths that have, in general, $f_j \neq 0$ and $z_j \neq 0$.

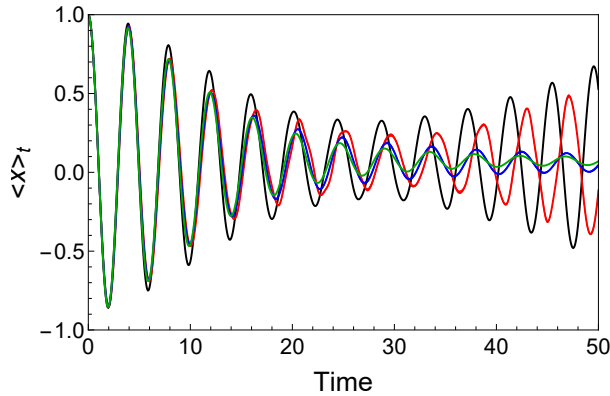


FIG. 12. The FFPI position correlation function for a 1D anharmonic oscillator calculated using our approximate classical-trajectory based implementation is shown for $c = 0$ (red), $c = 10^{-2}$ (blue), along with LSC-IVR results (green) and exact path integral results (black).

Numerical implementation challenges arise from the third type of path, and indeed represent the challenge in undertaking any high-dimensional exact real-time path integral simulation. In Fig. 12, we show the position correlation function obtained when we approximately calculate the FFPI correlation function limiting ourselves to only the first two types of classical paths. By design, this implementation does indeed correctly reproduce the classical limit LSC-IVR results,

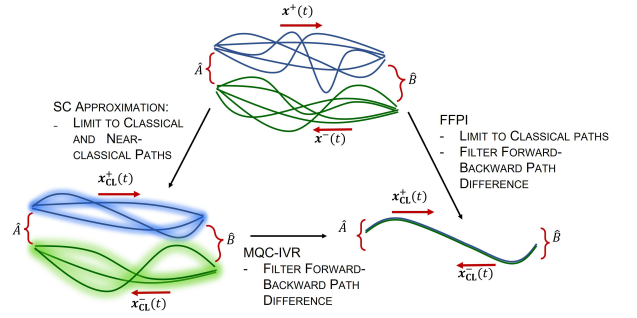


FIG. 13. We sketch a cartoon representing *all* forward, $x^+(t)$, and backward, $x^-(t)$, paths that contribute to the real-time correlation function $C_{AB}(t)$ in an exact path integral calculation. As described in the introduction, using the stationary phase approximation, it is possible to derive a quantum-limit SC approximation to the correlation function where only classical, $x_{CL}^\pm(t)$, and near-classical paths contribute. The MQC-IVR correlation function is obtained by Filinov filtering the difference in action between the forward and backward paths; in the limit of a strong filter, we obtain an expression where the paths coincide leading to a classical-limit SC result, the Husimi-IVR. In order to eliminate the SC prefactor, we derive the FFPI expression by simultaneously filtering contributions from non-classical paths and placing constraints on the difference in action between the forward and backward paths. In the limit of a strong filter, the FFPI correlation function also leads to a classical-limit SC result, in this case, LSC-IVR.

but while the short-time amplitudes are correctly described in the quantum limit and some recurrence is observed, the amplitudes and frequencies do not agree well in the quantum limit. An improved implementation is the subject of ongoing work, but we note that devising a mixed-limit implementation where a small number of system degrees of freedom are described at the DVR-level of theory and the rest treated in the classical-limit SC level of theory corresponds very closely to the Quantum-Classical Path Integral method^{164,165}.

III. CONCLUSIONS

We make the case that a rigorous SC framework for mixed quantum-classical simulations offers a balanced approach to large system simulations, retaining the ability to capture important quantum effects at a reduced cost by mitigating the sign problem. We derived the MQC-IVR expression for real-time correlation functions using the MFF scheme to damp the phase of a quantum limit correlation function and verify that changing the strength of Filinov parameter systematically changes the correlation function from quantum-limit DHK-IVR to the classical-limit Husimi IVR for linear operators. Further, we demonstrate the efficacy of mixed-limit MQC-IVR implementations for high-dimensional systems where quantizing a few degrees of freedom is typically sufficient to capture quantum effects. We show that several factors influence the choice of which modes to treat in the quantum limit including the nature of operator \hat{B} and inter-mode coupling strength.

While MQC-IVR offers an accurate framework when \hat{B} is a linear operator, for non-linear operators, the classical-limit can be incorrect even at time zero.¹⁶⁶ In a manuscript currently under preparation we address this limitation and offer some strategies to correct for the difference between the classical-limit MQC-IVR and the Husimi-IVR correlation function. In addition, we note that while there is significant improvement over DHK-IVR, the presence of a full dimensional SC prefactor remains a computational challenge to be overcome. In the mixed-limit AMQC-IVR, we offer a potential solution through a separable prefactor approximation. In addition, we note that many advances in approximating the SC prefactor have been made^{39–41,124,140–145} and several of these ideas may be employed in the context of MQC-IVR.

Finally, we introduce the FFPI framework to achieve a prefactor-free expression for real-time correlation functions. The connections between the exact real-time path integral expression, MQC-IVR, FFPI, and LSC-IVR are summarized in Fig. 13. Constructing a classical trajectory-based approach for path sampling the FFPI correlation function remains an outstanding challenge and one that we intend to explore through both more traditional path sampling strategies and through data-driven strategies.

ACKNOWLEDGMENTS

The authors would like to acknowledge prior postdoctoral researchers, graduate and undergraduate students who contributed to the previously published work described in this feature, particularly Dr. Sergey Antipov. N. A. and S. M. acknowledge funding from NSF CAREER Grant No. CHE 1555205.

Appendix A: MQC-IVR Prefactor

The MQC-IVR prefactor derived for the Forward-Backward implementation for a general operator \hat{B} is,

$$\begin{aligned}
D &= 2^{-\frac{N}{2}} \det(\gamma_0^{-1} \mathbf{G})^{\frac{1}{2}} \\
&\times \det \left[\frac{1}{2} (\mathbf{M}_{pp}^b - i\gamma_0 \mathbf{M}_{qp}^b) (\mathbf{G}^{-1} + \mathbb{1}) (\mathbf{M}_{pp}^f \gamma_0 + i\mathbf{M}_{pq}^f) \right. \\
&+ (\gamma_0 \mathbf{M}_{qq}^b + i\mathbf{M}_{pq}^b) \left(\frac{1}{2} \gamma_0^{-1} + \mathbf{c}_p \right) \mathbf{G}^{-1} (\mathbf{M}_{pp}^f \gamma_0 + i\mathbf{M}_{pq}^f) \\
&+ \frac{1}{2} (\gamma_0 \mathbf{M}_{qq}^b + i\mathbf{M}_{pq}^b) (\mathbf{G}^{-1} + \mathbb{1}) (\mathbf{M}_{qq}^f - i\mathbf{M}_{qp}^f \gamma_0) \\
&\left. + (\mathbf{M}_{pp}^b - i\gamma_0 \mathbf{M}_{qp}^b) \left(\frac{1}{2} \gamma_0 + \mathbf{c}_q \right) \mathbf{G}^{-1} (\mathbf{M}_{qq}^f - i\mathbf{M}_{qp}^f \gamma_0) \right]^{\frac{1}{2}}, \tag{A1}
\end{aligned}$$

where the diagonal matrix $\mathbf{G} = (\mathbf{c}_q + \gamma_0) \mathbf{c}_p + \mathbf{c}_q (\gamma_0^{-1} + \mathbf{c}_p)$.

Appendix B: Deriving the FFPI correlation function-IVR Prefactor

Once the choice of phase to be filtered is established [Eq. (21)], its derivatives can be evaluated to be,

$$\frac{\partial \phi(\mathbf{r})}{\partial \mathbf{r}} = -\frac{1}{\hbar} \mathbf{K} \cdot \mathbf{r} \quad \& \quad \frac{\partial^2 \phi(\mathbf{r})}{\partial \mathbf{r}^2} = -\frac{1}{\hbar} \mathbf{K}, \tag{B1}$$

where the constant block diagonal matrix \mathbf{K} is,

$$\mathbf{K} = \begin{pmatrix} 0 & 1 & \dots & \dots & \dots \\ 1 & 0 & \dots & \dots & \dots \\ \vdots & \vdots & \ddots & \vdots & \vdots \\ \dots & \dots & \dots & 0 & 1 \\ \dots & \dots & \dots & 1 & 0 \end{pmatrix}_{2(N-1) \times 2(N-1)}. \tag{B2}$$

The diagonal matrix of Filinov parameters is defined as

$$\mathbf{c} = \begin{pmatrix} c_{z_1} & \dots & \dots & \dots & \dots & \dots & \dots \\ \dots & c_{f_1} & \dots & \dots & \dots & \dots & \dots \\ \dots & \dots & c_{z_2} & \dots & \dots & \dots & \dots \\ \dots & \dots & \dots & c_{f_2} & \dots & \dots & \dots \\ \vdots & \vdots & \vdots & \vdots & \ddots & \vdots & \vdots \\ \dots & \dots & \dots & \dots & \dots & c_{z_{N-1}} & \dots \\ \dots & \dots & \dots & \dots & \dots & \dots & c_{f_{N-1}} \end{pmatrix}_{2(N-1) \times 2(N-1)}. \tag{B3}$$

- ¹W. H. Miller, *Journal of Physical Chemistry A* **105**, 2942 (2001).
- ²D. J. Tannor and S. Garashchuk, *Annual Review of Physical Chemistry* **51**, 553 (2000).
- ³M. Thoss and H. Wang, *Annual Review of Physical Chemistry* **55**, 299 (2004).
- ⁴K. G. Kay, *Annual Review of Physical Chemistry* **56**, 255 (2005).
- ⁵G. Stock and M. Thoss, in *Advances in Chemical Physics*, Vol. 131 (John Wiley & Sons, Ltd, 2005) pp. 243–375.
- ⁶E. J. Heller, *Accounts of Chemical Research* **39**, 127 (2006).
- ⁷R. Kapral, *Annual Review of Physical Chemistry* **57**, 129 (2006).
- ⁸E. Pollak, *Springer Series in Chemical Physics* **83**, 259 (2007).
- ⁹W. H. Miller, *Journal of Physical Chemistry A* **113**, 1405 (2009).
- ¹⁰P. L. McRobbie, G. Hanna, Q. Shi, and E. Geva, *Accounts of Chemical Research* **42**, 1299 (2009).
- ¹¹J. Liu, *International Journal of Quantum Chemistry* **115**, 657 (2015).
- ¹²M. K. Lee, P. Huo, and D. F. Coker, *Annual Review of Physical Chemistry* **67**, 639 (2016).
- ¹³J.-T. Lü, B.-Z. Hu, P. Hedegård, and M. Brandbyge, *Progress in Surface Science* **94**, 21 (2019), arXiv:1712.03863.
- ¹⁴R. Conte and M. Ceotto, in *Quantum Chemistry and Dynamics of Excited States* (Wiley, 2020) Chap. 19, pp. 595–628.
- ¹⁵M. Bonfanti, G. A. Worth, and I. Burghardt, in *Quantum Chemistry and Dynamics of Excited States* (Wiley, 2020) pp. 383–411.
- ¹⁶J. Vaníček and T. Begušić, *Molecular Spectroscopy and Quantum Dynamics*, 199 (2021).
- ¹⁷R. F. Loring, *Annual Review of Physical Chemistry* **73**, 273 (2022).
- ¹⁸C. Venkataraman and W. H. Miller, *The Journal of Chemical Physics* **126**, 094104 (2007).
- ¹⁹X. Sun, H. Wang, and W. H. Miller, *Journal of Chemical Physics* **109**, 4190 (1998).
- ²⁰H. Wang, X. Sun, and W. H. Miller, *Journal of Chemical Physics* **108**, 9726 (1998).
- ²¹Q. Shi and E. Geva, *Journal of Physical Chemistry A* **107**, 9059 (2003).
- ²²K. J. Being, Q. Shi, and E. Geva, *Journal of Physical Chemistry A* **109**, 5527 (2005).

- ²³I. Navrotskaya and E. Geva, *Journal of Physical Chemistry A* **111**, 460 (2006).
- ²⁴K. J. Being and E. Geva, *Journal of Physical Chemistry A* **110**, 13131 (2006).
- ²⁵K. J. Being and E. Geva, *Journal of Physical Chemistry A* **110**, 9555 (2006).
- ²⁶F. X. Vázquez, I. Navrotskaya, and E. Geva, *Journal of Physical Chemistry A* **114**, 5682 (2010).
- ²⁷H. Wang, M. Thoss, and W. H. Miller, *Journal of Chemical Physics* **112**, 47 (2000).
- ²⁸F. Grossmann, *Physical Review Letters* **85**, 903 (2000).
- ²⁹J. C. Burant and V. S. Batista, *The Journal of Chemical Physics* **116**, 2748 (2002).
- ³⁰M. A. Sepúlveda and F. Grossmann, in *Advances in Chemical Physics*, Vol. 96 (John Wiley & Sons, Ltd, 1996) pp. 191–304.
- ³¹J. Liu, W. H. Miller, G. S. Fanourgakis, S. S. Xantheas, S. Imoto, and S. Saito, *The Journal of Chemical Physics* **135**, 244503 (2011).
- ³²J. A. Poulsen, G. Nyman, and P. J. Rossky, *Proceedings of the National Academy of Sciences* **102**, 6709 (2005).
- ³³J. A. Poulsen, G. Nyman, and P. J. Rossky, *Journal of Chemical Theory and Computation* **2**, 1482 (2006).
- ³⁴J. Beutier, R. Vuilleumier, S. Bonella, and G. Ciccotti, *Molecular Physics* **113**, 2894 (2015).
- ³⁵A. L. Kaledin and W. H. Miller, *The Journal of Chemical Physics* **118**, 7174 (2003).
- ³⁶A. L. Kaledin and W. H. Miller, *The Journal of Chemical Physics* **119**, 3078 (2003).
- ³⁷A. L. Kaledin, X. Huang, and J. M. Bowman, *Chemical Physics Letters* **384**, 80 (2004).
- ³⁸O. Kühn and N. Makri, *The Journal of Physical Chemistry A* **103**, 9487 (1999).
- ³⁹B. B. Issack and P.-N. Roy, *The Journal of Chemical Physics* **127**, 054105 (2007).
- ⁴⁰S. Y. Y. Wong, D. M. Benoit, M. Lewerenz, A. Brown, and P.-N. Roy, *The Journal of Chemical Physics* **134**, 094110 (2011).
- ⁴¹G. D. Liberto and M. Ceotto, *The Journal of Chemical Physics* **145**, 144107 (2016).
- ⁴²M. Ceotto, S. Atahan, S. Shim, G. F. Tantardini, and A. Aspuru-Guzik, *Physical Chemistry Chemical Physics* **11**, 3861 (2009).
- ⁴³M. Ceotto, S. Atahan, G. F. Tantardini, and A. Aspuru-Guzik, *The Journal of Chemical Physics* **130**, 234113 (2009).
- ⁴⁴M. Ceotto, D. Dell’Angelo, and G. F. Tantardini, *The Journal of Chemical Physics* **133**, 054701 (2010).
- ⁴⁵R. Conte, A. Aspuru-Guzik, and M. Ceotto, *Journal of Physical Chemistry Letters* **4**, 3407 (2013).
- ⁴⁶F. Gabas, R. Conte, and M. Ceotto, *Journal of Chemical Theory and Computation* **13**, 2378 (2017).
- ⁴⁷M. Ceotto, S. Valteau, G. F. Tantardini, and A. Aspuru-Guzik, *The Journal of Chemical Physics* **134**, 234103 (2011).
- ⁴⁸C. Aieta, G. Bertaina, M. Micciarelli, and M. Ceotto, *The Journal of Chemical Physics* **153**, 214117 (2020).
- ⁴⁹C. Aieta, M. Micciarelli, G. Bertaina, and M. Ceotto, *Nature Communications* **11**, 1 (2020).
- ⁵⁰M. Micciarelli, F. Gabas, R. Conte, and M. Ceotto, *The Journal of Chemical Physics* **150**, 184113 (2019).
- ⁵¹M. Ceotto, G. D. Liberto, and R. Conte, *Physical Review Letters* **119**, 010401 (2017).
- ⁵²G. D. Liberto, R. Conte, and M. Ceotto, *The Journal of Chemical Physics* **148**, 014307 (2018).
- ⁵³G. D. Liberto, R. Conte, and M. Ceotto, *The Journal of Chemical Physics* **148**, 104302 (2018).
- ⁵⁴F. Gabas, G. D. Liberto, R. Conte, and M. Ceotto, *Chemical Science* **9**, 7894 (2018).
- ⁵⁵F. Gabas, G. D. Liberto, and M. Ceotto, *The Journal of Chemical Physics* **150**, 224107 (2019).
- ⁵⁶G. Bertaina, G. D. Liberto, and M. Ceotto, *The Journal of Chemical Physics* **151**, 114307 (2019).
- ⁵⁷M. Gandolfi, A. Rognoni, C. Aieta, R. Conte, and M. Ceotto, *The Journal of Chemical Physics* **153**, 204104 (2020).
- ⁵⁸M. Ovchinnikov and V. A. Apkarian, *Journal of Chemical Physics* **105**, 10312 (1996).
- ⁵⁹M. Ovchinnikov and V. A. Apkarian, *The Journal of Chemical Physics* **106**, 5775 (1998).
- ⁶⁰F. Grossmann, *Physica Scripta* **91**, 044004 (2016).
- ⁶¹M. Buchholz, C.-M. Goletz, F. Grossmann, B. Schmidt, J. Heyda, and P. Jungwirth, *Journal of Physical Chemistry A* **116**, 11199 (2012).
- ⁶²M. Buchholz, F. Grossmann, and M. Ceotto, *The Journal of Chemical Physics* **144**, 094102 (2016).
- ⁶³M. Buchholz, F. Grossmann, and M. Ceotto, *The Journal of Chemical Physics* **147**, 164110 (2017).
- ⁶⁴M. Buchholz, F. Grossmann, and M. Ceotto, *The Journal of Chemical Physics* **148**, 114107 (2018).
- ⁶⁵X. Sun and W. H. Miller, *The Journal of Chemical Physics* **106**, 6346 (1997).
- ⁶⁶X. Sun, H. Wang, and W. H. Miller, *The Journal of Chemical Physics* **109**, 7064 (1998).
- ⁶⁷V. S. Batista and W. H. Miller, *The Journal of Chemical Physics* **108**, 498 (1998).
- ⁶⁸E. Rabani, S. A. Egorov, and B. J. Berne, *The Journal of Physical Chemistry A* **103**, 9539 (1999).
- ⁶⁹H. Wang, X. Song, D. Chandler, and W. H. Miller, *The Journal of Chemical Physics* **110**, 4828 (1999).
- ⁷⁰M. Thoss, W. H. Miller, and G. Stock, *The Journal of Chemical Physics* **112**, 10282 (2000).
- ⁷¹Q. Shi and E. Geva, *Journal of Physical Chemistry A* **108**, 6109 (2004).
- ⁷²Q. Shi and E. Geva, *The Journal of Chemical Physics* **122**, 064506 (2005).
- ⁷³S. Bonella, D. Montemayor, and D. F. Coker, *Proceedings of the National Academy of Sciences of the United States of America* **102**, 6715 (2005).
- ⁷⁴N. Ananth. C. Venkataraman, and W. H. Miller, *The Journal of Chemical Physics* **127**, 084114 (2007).
- ⁷⁵Q. Shi and E. Geva, *The Journal of Chemical Physics* **129**, 124505 (2008).
- ⁷⁶W. H. Miller and G. Tao, *Journal of Physical Chemistry Letters* **1**, 891 (2010).
- ⁷⁷C. Venkataraman, *The Journal of Chemical Physics* **135**, 204503 (2011).
- ⁷⁸P. Huo and D. F. Coker, *The Journal of Chemical Physics* **135**, 201101 (2011).
- ⁷⁹P. Huo and D. F. Coker, *The Journal of Chemical Physics* **137**, 22A535 (2012).
- ⁸⁰S. J. Cotton and W. H. Miller, *The Journal of Chemical Physics* **139**, 234112 (2013).
- ⁸¹G. Tao, *Journal of Physical Chemistry A* **117**, 5821 (2013).
- ⁸²X. Sun and E. Geva, *Journal of Physical Chemistry A* **120**, 2976 (2015).
- ⁸³X. Sun and E. Geva, *Journal of Chemical Theory and Computation* **12**, 2926 (2016).
- ⁸⁴X. Sun and E. Geva, *The Journal of Chemical Physics* **144**, 244105 (2016).
- ⁸⁵X. Sun and E. Geva, *The Journal of Chemical Physics* **145**, 064109 (2016).
- ⁸⁶H.-H. Teh and Y.-C. Cheng, *The Journal of Chemical Physics* **146**, 144105 (2017).
- ⁸⁷A. A. Kananenka, X. Sun, A. Schubert, B. D. Dunietz, and E. Geva, *The Journal of Chemical Physics* **148**, 102304 (2017).
- ⁸⁸X. Sun, P. Zhang, Y. Lai, K. L. Williams, M. S. Cheung, B. D. Dunietz, and E. Geva, *The Journal of Physical Chemistry C* **122**, 11288 (2018).
- ⁸⁹J. Provazza, F. Segatta, M. Garavelli, and D. F. Coker, *Journal of Chemical Theory and Computation* **14**, 856 (2018).
- ⁹⁰J. Provazza and D. F. Coker, *The Journal of Chemical Physics* **151**, 154114 (2019).
- ⁹¹E. Mulvihill, X. Gao, Y. Liu, A. Schubert, B. D. Dunietz, and E. Geva, *The Journal of Chemical Physics* **151**, 074103 (2019).
- ⁹²X. Gao, M. A. C. Saller, Y. Liu, A. Kelly, J. O. Richardson, and E. Geva, *Journal of Chemical Theory and Computation* **16**, 2883 (2020).
- ⁹³X. Gao and E. Geva, *Journal of Physical Chemistry A* **124**, 11006 (2020).
- ⁹⁴A. Dodin, J. Provazza, D. F. Coker, and A. P. Willard, *Journal of Chemical Theory and Computation* **18**, 2047 (2022).
- ⁹⁵M. Kumar, J. Provazza, and D. F. Coker, *The Journal of Chemical Physics* **154**, 224109 (2021).
- ⁹⁶R. P. Feynman and A. R. Hibbs, *Quantum Mechanics and Path Integrals* (McGraw-Hill, 1965).
- ⁹⁷J. H. Van Vleck, *Proceedings of the National Academy of Sciences* **14**, 178 (1928).

- ⁹⁸W. H. Miller, *The Journal of Chemical Physics* **53**, 3578 (1970).
- ⁹⁹E. J. Heller, *Journal of Chemical Physics* **94**, 2723 (1991).
- ¹⁰⁰E. J. Heller, *Journal of Chemical Physics* **95**, 9431 (1991).
- ¹⁰¹W. H. Miller, *The Journal of Chemical Physics* **95**, 9428 (1991).
- ¹⁰²M. F. Herman and E. Kluk, *Chemical Physics* **91**, 27 (1984).
- ¹⁰³X. Sun and W. H. Miller, *Journal of Chemical Physics* **106**, 916 (1997).
- ¹⁰⁴Q. Shi and E. Geva, *The Journal of Chemical Physics* **118**, 8173 (2003).
- ¹⁰⁵Y. Zhao and N. Makri, *Chemical Physics* **280**, 135 (2002).
- ¹⁰⁶N. J. Wright and N. Makri, *Journal of Physical Chemistry B* **108**, 6816 (2004).
- ¹⁰⁷R. Gelabert, X. Giménez, M. Thoss, H. Wang, and W. H. Miller, *Journal of Chemical Physics* **114**, 2572 (2001).
- ¹⁰⁸J. Liu and W. H. Miller, *The Journal of Chemical Physics* **125**, 224104 (2006).
- ¹⁰⁹J. Liu and W. H. Miller, *The Journal of Chemical Physics* **127**, 114506 (2007).
- ¹¹⁰J. Liu and W. H. Miller, *The Journal of Chemical Physics* **128**, 144511 (2008).
- ¹¹¹J. Liu, B. J. Alder, and W. H. Miller, *The Journal of Chemical Physics* **135**, 114105 (2011).
- ¹¹²M. Monteferrante, S. Bonella, and G. Ciccotti, *The Journal of Chemical Physics* **138**, 054118 (2013).
- ¹¹³J. A. Poulsen, G. Nyman, and P. J. Rossky, *Journal of Chemical Physics* **119**, 12179 (2003).
- ¹¹⁴J. A. Poulsen, G. Nyman, and P. J. Rossky, *Journal of Physical Chemistry B* **108**, 19799 (2004).
- ¹¹⁵J. A. Poulsen, G. Nyman, and P. J. Rossky, *Journal of Physical Chemistry A* **108**, 8743 (2004).
- ¹¹⁶J. A. Poulsen, J. Scheers, G. Nyman, and P. J. Rossky, *Physical Review B* **75**, 224505 (2007).
- ¹¹⁷F. Pan and G. Tao, *The Journal of Chemical Physics* **138**, 091101 (2013).
- ¹¹⁸G. Tao and W. H. Miller, *The Journal of Chemical Physics* **135**, 024104 (2011).
- ¹¹⁹G. Tao and W. H. Miller, *The Journal of Chemical Physics* **137**, 124105 (2012).
- ¹²⁰G. Tao and W. H. Miller, *Molecular Physics* **111**, 1987 (2013).
- ¹²¹G. Tao, *Theoretical Chemistry Accounts* **133**, 1448 (2014).
- ¹²²Y. Elran and K. G. Kay, *The Journal of Chemical Physics* **110**, 3653 (1999).
- ¹²³Y. Elran and K. G. Kay, *The Journal of Chemical Physics* **110**, 8912 (1999).
- ¹²⁴B. B. Issack and P.-N. Roy, *The Journal of Chemical Physics* **127**, 144306 (2007).
- ¹²⁵N. Makri and K. Thompson, *Chemical Physics Letters* **291**, 101 (1998).
- ¹²⁶K. Thompson and N. Makri, *Physical Review E* **59**, R4729 (1999).
- ¹²⁷K. Thompson and N. Makri, *The Journal of Chemical Physics* **110**, 64112 (1999).
- ¹²⁸A. Nakayama and N. Makri, *The Journal of Chemical Physics* **119**, 8592 (2003).
- ¹²⁹N. J. Wright and N. Makri, *The Journal of Chemical Physics* **119**, 1634 (2003).
- ¹³⁰N. Makri, A. Nakayama, and N. J. Wright, *Journal of Theoretical and Computational Chemistry* **3**, 391 (2004).
- ¹³¹C. P. Lawrence, A. Nakayama, N. Makri, and J. L. Skinner, *The Journal of Chemical Physics* **120**, 6621 (2004).
- ¹³²N. Makri, *Phys. Chem. Chem. Phys* **13**, 14442 (2011).
- ¹³³G. Tao and W. H. Miller, *The Journal of Chemical Physics* **130**, 184108 (2009).
- ¹³⁴F. Grossmann, *The Journal of Chemical Physics* **125**, 014111 (2006).
- ¹³⁵C.-M. Goletz and F. Grossmann, *The Journal of Chemical Physics* **130**, 244107 (2009).
- ¹³⁶C. M. Goletz, W. Koch, and F. Grossmann, *Chemical Physics* **375**, 227 (2010).
- ¹³⁷E. J. Heller, *The Journal of Chemical Physics* **62**, 1544 (1975).
- ¹³⁸R. G. Littlejohn, *Physics Reports* **138**, 193 (1986).
- ¹³⁹S. A. Deshpande and G. S. Ezra, *Journal of Physics A: Mathematical and General* **39**, 5067 (2006).
- ¹⁴⁰R. Gelabert, X. Giménez, M. Thoss, H. Wang, and W. H. Miller, *Journal of Physical Chemistry A* **104**, 10321 (2000).
- ¹⁴¹B. B. Issack and P.-N. Roy, *The Journal of Chemical Physics* **123**, 084103 (2005).
- ¹⁴²B. B. Issack and P.-N. Roy, *The Journal of Chemical Physics* **126**, 024111 (2007).
- ¹⁴³V. Guallar, V. S. Batista, and W. H. Miller, *Journal of Chemical Physics* **110**, 9922 (1999).
- ¹⁴⁴V. Guallar, V. S. Batista, and W. H. Miller, *The Journal of Chemical Physics* **113**, 9510 (2000).
- ¹⁴⁵J. Tatchen, E. Pollak, G. Tao, and W. H. Miller, *The Journal of Chemical Physics* **134**, 134104 (2011).
- ¹⁴⁶S. Zhang and E. Pollak, *Journal of Chemical Physics* **121**, 3384 (2004).
- ¹⁴⁷E. Pollak and J. Shao, *Journal of Physical Chemistry A* **107**, 7112 (2003).
- ¹⁴⁸S. Zhang and E. Pollak, *Physical Review Letters* **91**, 190201 (2003).
- ¹⁴⁹S. Zhang and E. Pollak, *The Journal of Chemical Physics* **119**, 11058 (2003).
- ¹⁵⁰S. V. Antipov, Z. Ye, and N. Ananth, *The Journal of Chemical Physics* **142**, 184102 (2015).
- ¹⁵¹M. S. Church, S. V. Antipov, and N. Ananth, *The Journal of Chemical Physics* **146**, 234104 (2017).
- ¹⁵²M. S. Church and N. Ananth, *The Journal of Chemical Physics* **151**, 134109 (2019).
- ¹⁵³M. S. Church, T. J. H. Hele, G. S. Ezra, and N. Ananth, *The Journal of Chemical Physics* **148**, 102326 (2018).
- ¹⁵⁴V. Filinov, *Nuclear Physics B* **271**, 717 (1986).
- ¹⁵⁵N. Makri and W. H. Miller, *Chemical Physics Letters* **139**, 10 (1987).
- ¹⁵⁶N. Makri and W. H. Miller, *The Journal of Chemical Physics* **89**, 2170 (1988).
- ¹⁵⁷M. Thoss, H. Wang, and W. H. Miller, *The Journal of Chemical Physics* **114**, 9220 (2001).
- ¹⁵⁸Sc-corr: open-source software for the calculation of sc-ivr and sc-ivr based approximations to quantum real-time correlation functions.
- ¹⁵⁹D. T. Colbert and W. H. Miller, *J. Chem. Phys.* **96**, 1982 (1992).
- ¹⁶⁰H. D. Meyer and W. H. Miller, *The Journal of Chemical Physics* **70**, 3214 (1979).
- ¹⁶¹G. Stock and M. Thoss, *Physical Review Letters* **78**, 578 (1997).
- ¹⁶²A. Kelly, R. van Zon, J. Schofield, and R. Kapral, *The Journal of Chemical Physics* **136**, 084101 (2012).
- ¹⁶³M. Topaler and N. Makri, *Journal of Chemical Physics* **101**, 7500 (1994).
- ¹⁶⁴R. Lambert and N. Makri, *Journal of Chemical Physics* **137**, 22A552 (2012).
- ¹⁶⁵R. Lambert and N. Makri, *Journal of Chemical Physics* **137**, 22A553 (2012).
- ¹⁶⁶S. Loho Choudhury and F. Großmann, *Condensed Matter* **5**, 3 (2020).